THE JOURNAL OF PHYSICAL CHEMISTRY C

Article

Cite This: J. Phys. Chem. C 2019, 123, 3180−3187

pubs.acs.org/JPCC

Predicting the Electrochemical Synthesis of 2D Materials from First Principles

Michael Ashton,[†] Nicole Trometer,[†] Kiran Mathew,[∥] Jin Suntivich,[∥] Christoph Freysoldt,[§] Susan B. Sinnott,[⊥] and Richard G. Hennig*,[‡]

[†]Department of Materials Science and Engineering and [‡]Department of Materials Science and Engineering, University of Florida, Gainesville, Florida 32611-6400, United States

[§]Max-Planck-Institut für Eisenforschung, Max-Planck-Straße 1, Düsseldorf 40227, Germany

[∥]Department of Materials Science and Engineering, Cornell University, Ithaca, New York 14850, United States

[⊥]Department of Materials Science and Engineering, The Pennsylvania State University, University Park, Pennsylvania 16801-7003, United States

ABSTRACT: We show that Pourbaix diagrams generated by combining first principles and tabulated experimental data can determine the electrochemical conditions needed to synthesize metastable phases in solution. As an example, we investigate the synthesis of two-dimensional transition-metal carbides and nitrides (M_2Xenes) from their M_2AX phase precursors and observe good agreement between the predicted synthesis conditions and those used for existing M_2Xenes. In addition, we prescribe synthesis conditions to increase the yields of certain M_2Xenes and possibly even enable the synthesis of new M_2Xenes. Our results show that the general stability of nitride M_2Xenes is not dramatically different from their carbide counterparts, but that most of their experimentally available precursors are more difficult to etch initially because of their more inert A elements.

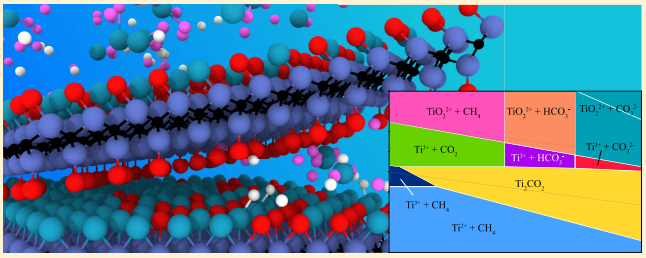

■ INTRODUCTION

Acid etching is one of several techniques available for creating two-dimensional (2D) materials.[1−4] This process is typically performed by immersing a layered bulk precursor in an acid chosen to selectively remove layers of sacrificial atomic species from among other layers. The newly exposed surfaces of the remaining 2D layers might be passivated by species in solution,[5] and often bind to one another through weak dispersion forces.[6]

Theory and modeling have become indispensable tools for predicting the stability of new 2D materials[7−11] and their synthesis through methods like mechanical exfoliation[12,13] or chemical vapor deposition.[14,15] For synthesis via acid etching, the aqueous environment presents additional challenges for accurate modeling by first-principles approaches.[16,17]

Here, we present a first-principles framework to characterize the acid etching process of bulk precursor compounds and predict the synthesis conditions for the formation of 2D materials. Our consideration includes applied electric potentials, which are often ignored as a degree of freedom during experimental synthesis. This allows us to investigate the effects of the chosen acid and its concentration, the potential in solution, and the choice of the bulk precursor compound from first-principles calculations. As a benchmark and example of the framework's usage, we investigate the synthesis of several MXenes, a well-studied class of 2D materials that has been synthesized by acid etching.[5,6,8,18−25]

■ MXENES

MXenes are 2D transition-metal carbides and nitrides that can be etched from layered ceramics known as MAX phases.[26−30] These ceramics derive their name from their chemical formula $M_{n+1}AX_n$, where M is an early transition metal, A a group 12−16 element, X carbon or nitrogen, and n generally ranges from 1 to 3. The specific cases discussed in this work are all for n = 1, and we will use the term M_2Xenes for this subclass. Figure 1a shows an example crystal structure for the V_2AlC MAX phase. Due to their compositional flexibility, the list of experimentally available MAX phases is quite large and growing.[31]

When certain MAX compounds are immersed in an aqueous HF solution or in other solvents with active F^- ions,[32,33] the acid selectively attacks the M−A bonds, often forming AF_x compounds, which diffuse out from among $M_{n+1}X_n$ layers. These $M_{n+1}X_n$ layers are immediately passivated by species coming from the solution, especially oxygen,[5] to form a final stoichiometry close to $M_{n+1}X_nO_2$. At this point during the

Received: November 6, 2018
Revised: January 14, 2019
Published: January 15, 2019

DOI: 10.1021/acs.jpcc.8b10802
J. Phys. Chem. C 2019, 123, 3180−3187

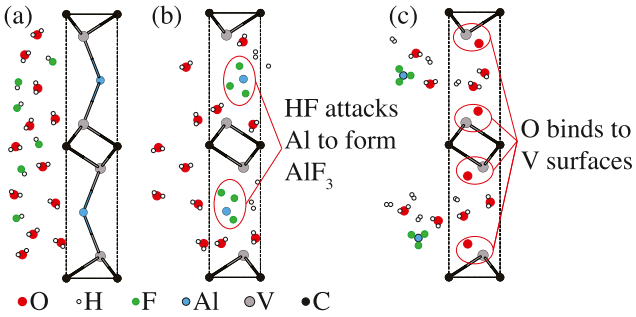

Figure 1. Illustration of the etching process for the V_2AlC M_2AX phase. (a) V_2AlC crystal structure is immersed in an aqueous 0.5 M HF solution. (b) F^- ions sever the V−Al bonds and are starting to form new Al−F bonds. (c) Etching is complete, with O atoms bound to the newly exposed V surfaces on the M_2Xene and Al−F ions or AlF_3 salts diffusing out.

synthesis, the $M_{n+1}X_nO_2$, or MXene, layers are held together by dispersion forces, and can be mechanically separated after removal from the solution. Not including compositions with solid solutions of more than one M or X element, the MXenes that have been successfully synthesized in this way include Ti_2CO_2, V_2CO_2, Nb_2CO_2, Ti_2NO_2, $Ti_3C_2O_2$, $Ti_4N_3O_2$, $Nb_4C_3O_2$, and $Ta_4C_3O_2$.[6,21,23,24,34−37] Mo_2CO_2, $Zr_3C_2O_2$, and $Hf_3C_2O_2$ MXenes have also been synthesized using slightly different precursors and/or techniques.[38−40]

METHODS

Recently, Persson et al.[16] developed a formalism to compare the formation energies of solids, molecules, and ions in solution by combining experimental data and density-functional theory (DFT), which provides a new theoretical microscope for investigations of aqueous etching processes. This formalism enables the construction of Pourbaix, or pE/pH phase, diagrams, which illustrate which species are thermodynamically stable in an aqueous solution at a given applied potential and pH. The formalism is briefly described in the next sections, and for a complete discussion along with validation of its accuracy, the reader is referred to ref 16.

This formalism has been coded into the Pymatgen software package,[41] which has a library of functions for creating Pourbaix diagrams. We have implemented this functionality for metastable phases in the MPInterfaces software package,[42] and it is this implementation that we use to create the diagrams in this work.

Using this approach, we construct Pourbaix diagrams to investigate the aqueous stability of several nonsolid solution $n = 1$ MXenes and their corresponding MAX phases, hereafter referred to as M_2Xenes and M_2AX phases, respectively. On the basis of these diagrams, we predict experimental etching solutions with the highest chance of successful synthesis for selected M_2Xenes.

Pourbaix Diagrams. To generate the Pourbaix diagrams for the M_2Xenes and M_2AX phases, we select known competing ionic and molecular species that may form in solution from experimental databases.[43,44] Only molecular and elemental species are considered; additional solid phases are intentionally left out since they have been considered as competing phases for MXenes elsewhere,[5] and molecular species represent the most kinetically straightforward decomposition products in solution. We utilize the experimental ionic formation energies obtained from the NIST NBS tables[43] in lieu of DFT-calculated values, as it is computationally very demanding to obtain reliable formation energies for dissolved ions and molecules in standard DFT. For dissolved species for which the NBS tables do not contain data, we use values from Pourbaix's 1966 Atlas.[44] We extract formation energies from these references for all molecules containing E−O, E−H, and E−O−H, where E is repeated for each of the M, A, and X elements. We also add molecules with compositions containing fluorine, since it is also present in the experimental etching solutions.

We employ the formation energies for standard conditions, G_i^0, to calculate the Gibbs free energy, G_i, of each species, i, in solution[45]

$$G_i(c_i, \mathrm{pH}, \phi) = G_i^0 + 0.0591 \log c_i - n_O\mu_{H_2O} + \mathrm{pH}\,(n_H - 2n_O) + \phi(-n_H + 2n_O + q_i) \quad (1)$$

where c_i is the concentration of species i, n_O and n_H are the respective numbers of oxygen and hydrogen atoms in the species, μ_{H_2O} is set to the formation energy of water at −2.46 eV, ϕ is the electric potential, and q_i is the species' charge. We select a moderate concentration of 10^{-3} M for all ionic species in solution unless otherwise noted, and include ions containing F to mimic the experimental solution. Equation 1 without the concentration-dependent term also describes the Gibbs free energy of the solid phases as a function of pH and applied potential, ϕ. From the Gibbs free energies of all dissolved species and solid phases, i, and their dependence on pH and potential, ϕ, we construct the Pourbaix diagram as the convex hull connecting the formation energies of all compounds and species, just like any other phase diagram.

DFT Calculations. The energies of all solid compounds are calculated using DFT with the Vienna ab initio simulation package (VASP).[46,47] To obtain an accuracy of about 1 meV/atom, we use a plane-wave basis with a cutoff energy of 500 eV and sample the reciprocal spaces with a Monkhorst−Pack mesh[48] with a density of 1000 k-points per atom.

While in solution, M_2Xenes exist as dispersion-bound multilayer structures and not free-standing nanosheets. Their accordion-like morphologies typically contain dozens of individual layers.[18] Therefore, the energies of the M_2Xenes are calculated using fully periodic structures[49] to account for the binding interaction among neighboring layers. Dispersion-corrected optB88 functionals[50−53] are used to accurately capture the interlayer interactions in these structures.

Correction to Experimental Formation Energies. To bridge the compatibility gap between experimental formation energies and DFT-calculated formation energies, we employ the linear correction scheme of Persson et al.[16] In this formalism, experimental formation energies of ions are shifted by the difference between the DFT and experimental formation energies of a reference compound (preferably a simple binary oxide) containing the same element as the ion. For example, the correction factor applied to the formation energies of all ions containing Nb is calculated as

$$\Delta\mu_{Nb}^{corr} = \frac{1}{2}[E_f^{DFT}(Nb_2O_5) - E_f^{exp}(Nb_2O_5)] \quad (2)$$

where Nb_2O_5 is the reference compound and the factor 1/2 normalizes the correction per Nb atom. The experimental formation energies, E_f^{exp}, are taken for all binary oxides from ref

DOI: 10.1021/acs.jpcc.8b10802
J. Phys. Chem. C 2019, 123, 3180−3187

54. We apply this correction additively for each atom in a molecule or molecular ion.

Potentials of Zero Charge. The intrinsic electric potential at a neutral metallic surface in solution, or the potential of zero charge (PZC), is often nonzero. This is an important effect to consider in etching processes because it can create local potentials at the precursor surface where the etching reactions occur, even when no external potential has been applied. Therefore, the PZC can be used to determine the relevant region of the Pourbaix diagram for an experimental etching reaction carried out without any external field.

To obtain PZC values for M_2AX surfaces, we calculate the Fermi level of M-terminated M_2AX slabs in an implicitly modeled solvent. The PZC is equal to the difference between the Fermi level of the slab and the potential in the bulk of the solvent with respect to the standard hydrogen electrode (SHE).

We use the implicit solvation model VASPsol[55,56] with an aqueous electrolyte of permittivity ϵ_r = 78.4 and a Debye length of 2 Å, and a slab thickness of 11 atomic layers, separated by 30 Å of the solvent. The SHE potential calculated using VASPsol is 4.6 V.[56] With these settings, we obtain the PZC values that are shown as horizontal dashed lines in the Pourbaix diagrams below.

Stability Criteria. The successful synthesis of a M_2Xene by electrochemical etching of a M_2AX phase requires two conditions to be fulfilled. First, the solution must be able to etch the A element from the M_2AX phase. This can be observed by the instability of the M_2AX phase in the Pourbaix diagram and the formation of A−F ions. These ions typically precipitate as AF_x salts during experimental synthesis, as illustrated in Figure 1. The second condition is that the remaining M_2XO_2 layers must not dissolve in the solution. In other words, the overall reaction should proceed as

$$M_2AX + 2H_2O + nHF \rightarrow M_2XO_2(\text{MXene}) + AF_n(s) + \left(\frac{4+n}{2}\right)H_2 \quad (3)$$

These two criteria can be investigated simultaneously by creating a Pourbaix diagram with the M_2AX phase and the M_2Xene as its only two solid phases. Any regions in this diagram where the M_2AX phase is unstable against dissolution and where the M_2Xene is stable against dissolution indicate conditions under which the synthesis reaction should proceed.

We refer to these partial Pourbaix diagrams that contain only the two solid phases of interest as "etching" diagrams to distinguish between them and complete Pourbaix diagrams that contain all thermodynamically stable solid phases. Diagrams of this nature can be generated to illustrate any electrochemical etching process for which the expected initial and final stable or metastable compounds are known.

■ RESULTS AND DISCUSSION

Benchmarking the Stability of Existing M_2Xenes. Figure 2 illustrates the application of this approach to the synthesis of the Ti_2CO_2 M_2Xene by electrochemical etching of the Ti_2AlC M_2AX precursor. Ti_2CO_2 has been experimentally synthesized by etching Ti_2AlC in aqueous HF solutions of 0.5 M concentration, which have a pH of about 1.5.[18] There is a large region of stability for Ti_2CO_2 in the diagram, indicating the wide range of conditions under which this 2D material is stable. Additionally, there are no solution conditions where the Ti_2AlC precursor will not be etched.

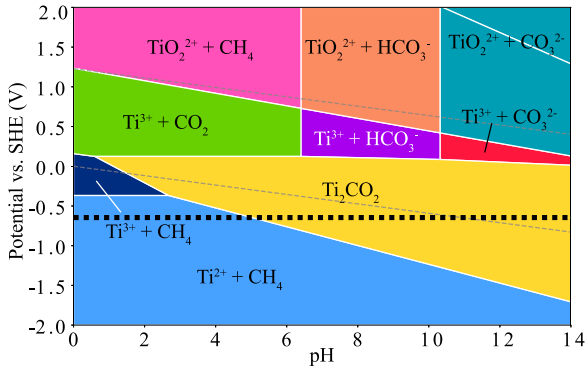

Figure 2. Etching diagram for Ti_2AlC, showing a region of stability for Ti_2CO_2. For clarity, only Ti- and C-containing ions are labeled in the diagrams. The composition including other ions (e.g., Al- and F-based ions) changes for every facet in the diagram (regions enclosed by the solid white lines). The dashed black line indicates the PZC, and the dashed gray lines indicate the stability range for water.

The experimental conditions (pH = 1.5 and 0 V applied potential) are very near to the left edge of the predicted Ti_2CO_2 stability region, but with the PZC value for this system around −0.6 V, we expect that Ti_2CO_2 may not immediately be stable in the experimental solution near the Ti_2AlC surface. This could explain why synthesis attempts have achieved only 60% Ti_2CO_2 yield. If we assume that the other 40% of the possible yield dissolves into solution, the ionic concentration and pH values in solution will increase as the etching progresses.

Figure 3 shows how the stability region for Ti_2CO_2 grows in size as the ionic concentration is increased from 10^{-5} to 10^{-1} M, following Le Châtelier's principle and eq 1. We therefore anticipate that Ti_2CO_2 becomes increasingly stable as the etching reaction progresses and that etching solutions preconditioned with high ion concentrations may increase Ti_2CO_2 yield.

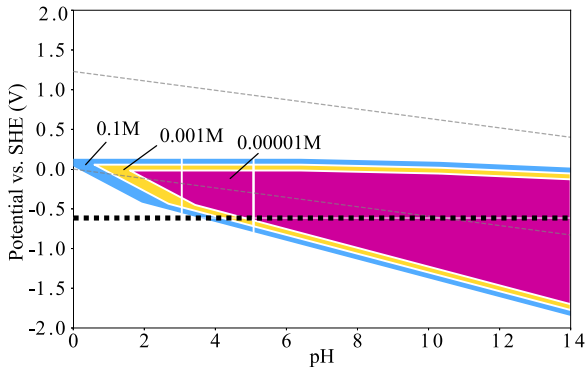

Figure 3. Regions of stability for Ti_2CO_2 at three different ion concentrations of 10^{-1}, 10^{-3}, and 10^{-5} M.

In addition to Ti_2CO_2, two other carbide M_2Xenes (not including solid solutions) have been synthesized from M_2AX phases to date: Nb_2CO_2 and V_2CO_2.[21] Both of these were etched from A = Al M_2AX phases.

The etching diagram for Nb_2CO_2 in Figure 4 shows a wide range of stability at negative potentials. At low pH, the potential where Nb_2CO_2 becomes stable (−0.6 V) is quite

DOI: 10.1021/acs.jpcc.8b10802
J. Phys. Chem. C 2019, 123, 3180−3187

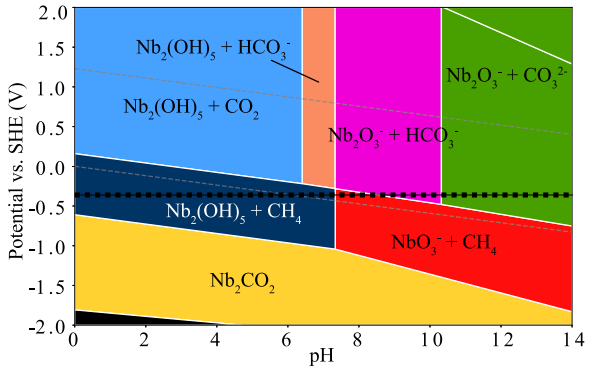

Figure 4. Etching diagram for Nb_2AlC with Nb_2CO_2. The PZC value is shown by the dashed black line.

close to its calculated PZC of −0.4 V, meaning that even without the application of an external potential, the reaction is expected to take place in 0.5 M HF solutions. This agrees well with the observed experimental yields of close to 100% for this M_2Xene.[21]

Figure 5a shows that V_2CO_2 is only stable at higher pH when using an ion concentration of 10^{-3} M. Similar to the case

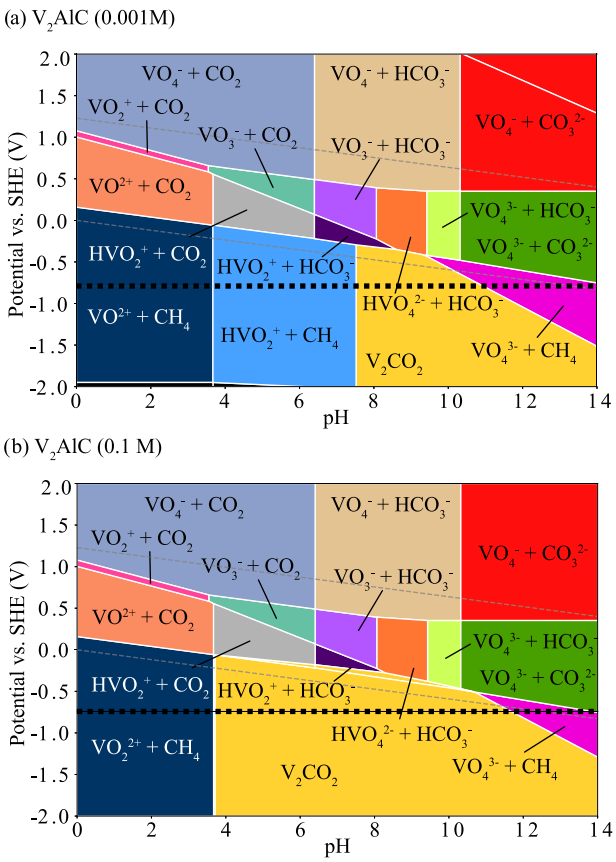

Figure 5. Etching diagrams for V_2AlC with V_2CO_2 at ion concentrations of (a) 10^{-3} M and (b) 10^{-1} M. The PZC value is shown by the dashed black line.

of Ti_2CO_2, this could explain why V_2CO_2 yields were only around 60% in the initial report of its synthesis.[21] Figure 5b shows the etching diagram for V_2CO_2 using projected experimental conditions after considerable dissolution; at an ion concentration of 0.1 M, the stability region for V_2CO_2 indeed spreads into acidic pH values between 3 and 4, reaffirming the reduced yield and delayed onset of successful etching for this material.

A small amount of the Mo_2CO_2 M_2Xene was synthesized[38] by etching a Mo_2Ga_2C nanolaminate[57] similar to the Mo_2GaC M_2AX phase. Mo_2GaC has not been successfully etched, so the exfoliation of Mo_2Ga_2C to form a M_2Xene nanosheet is a promising result, which broadens the possibilities of M_2Xene synthesis from off-stoichiometry $M_{n+1}AX_n$ phases.

The etching diagrams for Mo_2GaC and Mo_2Ga_2C in Figure 6 show that these precursors behave quite similarly and are

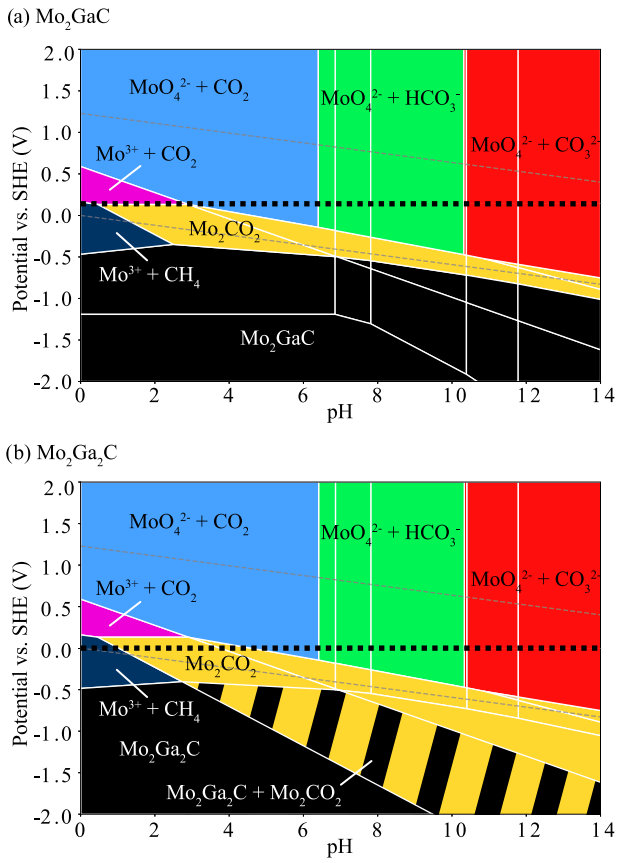

Figure 6. Etching diagrams including 2D Mo_2CO_2 for (a) Mo_2GaC and (b) Mo_2Ga_2C. The PZC values are shown by the dashed black lines.

more difficult to etch than the A = Al precursors shown so far. The main difference between these two is that there is a region in Figure 6b where Mo_2Ga_2C and Mo_2CO_2 are expected to coexist, but no such region exists for Mo_2GaC under the same conditions.

The actual Mo_2CO_2 yields were not provided in the report of its synthesis, but significant amounts of an unetched precursor were observed in the final solution along with Mo_2CO_2,[38] in good qualitative agreement with the coexistence region in Figure 6b. We also highlight that the PZC is slightly lower for Mo_2Ga_2C than for Mo_2GaC, which may also help to stabilize Mo_2CO_2 as it forms. Our results confirm that Mo_2Ga_2C is a better precursor than Mo_2GaC, but that 100% yields for either precursor may be difficult to achieve.

Our predictions for these systems indicate that these diagrams can capture successful experimental etching conditions with an estimated accuracy around pH ±1 and ±0.5 V.

DOI: 10.1021/acs.jpcc.8b10802
J. Phys. Chem. C 2019, 123, 3180−3187

This limit is most likely due to the kinetic barriers that can block the formation of solvated species like CH_4. For example, if the formation of CH_4 from Nb_2CO_2 is inhibited, the Nb_2CO_2 stability region in Figure 4 can expand even to within the stability range of water. Therefore, experimental conditions close to but not inside the predicted M_2Xene stability region may well be sufficient for successful etching.

Despite the good description of these benchmark systems, we point out that a number of experimental subtleties have not been treated by our DFT calculations, including the effects of varying surface coverage (species other than oxygen on the M_2Xene surfaces or incomplete surface coverage) on the M_2Xenes' stability. Effects of this nature can arise for varying potentials, pH, or pH_2.

Nitride M_2Xenes. The etching diagrams of nitride, or X = N, M_2Xenes are of particular interest because these materials are more difficult to synthesize.[24] Nitride M_2Xenes also have electronic and mechanical properties considerably different from their carbide counterparts,[24,58] meaning that their synthesis opens up a new range of accessible properties in the M_2Xene family. So far only two nitride MXenes, Ti_2NO_2[37] and $Ti_4N_3O_2$,[36] have been synthesized directly in solution, both from their A = Al MAX phases. The list of experimentally known nitride M_2AX phases includes Ti_2AlN, Ti_2GaN, Ti_2InN, V_2GaN, Cr_2GaN, Zr_2InN, Zr_2TlN, and Hf_2SnN. We calculate and show etching diagrams for Ti_2AlN and V_2GaN in Figure 7.

The etching diagram for Ti_2AlN in Figure 7a displays a large stability region for Ti_2NO_2. This does not immediately explain why Ti_2NO_2 could not originally be synthesized using 5, 10, or 20% HF solutions,[37,59] but it does indicate that this M_2Xene can exist as a metastable phase in acidic solutions. This is in agreement with later successful attempts at synthesis using hydrochloric acid and potassium fluoride.[59] The formation of anatase TiO_2 was observed in the unsuccessful synthesis attempts using HF etchants, meaning that nitride M_2Xenes must be carefully protected from excessive oxidation during synthesis. We have intentionally excluded TiO_2, which is known to be the ground state for titanium in water under most conditions, from our diagrams to show the possibility of metastable phases forming. If it is included, it replaces Ti_2NO_2 everywhere it appears in the diagram.

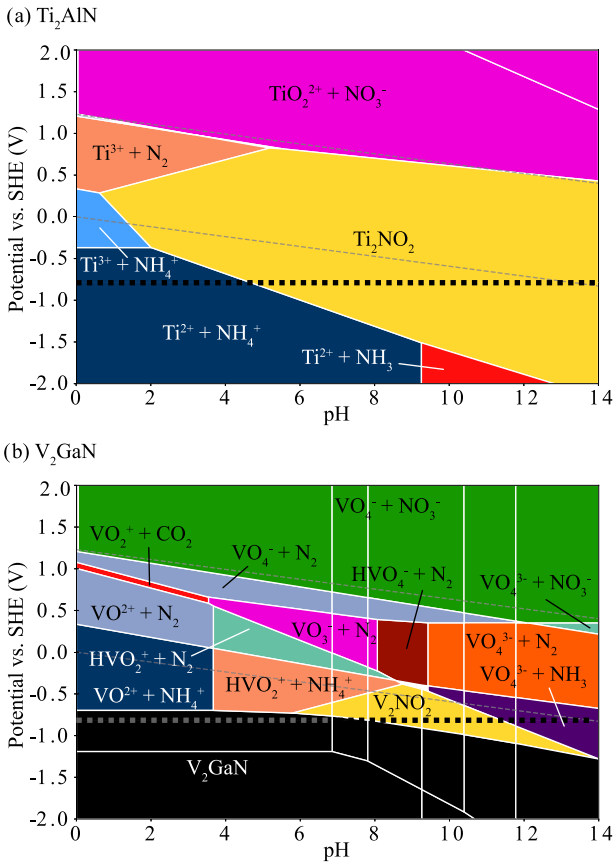

Figure 7. Etching diagrams for (a) Ti_2AlN and (b) V_2GaN and their respective M_2Xenes. The PZC values are shown by the dashed black lines.

Similar to Mo_2GaC, V_2GaN in Figure 7b still displays a large region of stability for the M_2AX phase at low potentials close to its calculated PZC where no etching is expected to occur. The appearance of this large M_2AX phase stability region for A ≠ Al is observed for other systems as well, confirming that A = Al M_2AX phases are generally the best precursors for etching. Unfortunately, Ti_2AlN is the only such X = N M_2AX phase currently in existence. We expect that the lack of A = Al precursors is at least partly responsible for the rarity of nitride M_2Xenes. We also note that V_2NO_2 and Mo_2NO_2 were very recently synthesized by ammoniation of their carbide M_2Xene counterparts,[58] a synthesis route that circumvents the need for an A = Al, X = N precursor and may prove to be successful for a number of other nitride M_2Xenes.

Aqueous Stability of New M_2Xenes. *Cr- and Ta-Based M_2Xenes.* Cr_2AlC exists as a precursor from which a new Cr_2CO_2 M_2Xene could potentially be synthesized.[27,60] The etching diagram generated for this system in Figure 8a shows only a small window of stability for Cr_2CO_2 at pH > 9. Similar to those of Ti_2CO_2 and V_2CO_2, this region grows with increasing ion concentration, but not as dramatically. Still, it is possible that some yield of Cr_2CO_2 could be achieved by carefully etching Cr_2AlC at moderate pH and high ion concentrations.

Ta_2AlC, in Figure 8b, displays a flat stability region for Ta_2CO_2 at potentials below −1.25 V and dissolves to form TaO_2^+ everywhere else in the diagram. The PZC for Ta_2AlC is actually slightly positive (0.08 V), so it is likely that an external potential would need to be applied to the solution to successfully etch Ta_2AlC into Ta_2CO_2. Such a strong potential is well outside the range of water's stability, however, and may therefore lead to other more complex dissociation processes.

Sc-, Zr-, and Hf-Based M_2Xenes. We find that no M_2Xenes based on Sc, Zr, and Hf have any stability against dissolution in their precursor etching diagrams, even at high ionic concentrations. For Sc-based M_2Xenes, the Sc atoms dissolve into solution to form Sc^{3+} ions at pH < 4 and $ScOH^{2+}$ ions at pH > 4. Zr atoms from Zr-based M_2Xenes are predicted to primarily form $HZrO_3^{3-}$ ions in solutions with negative potentials. Similarly, Hf atoms will readily form HfO^{2+} in solution. All of these dissolution reactions show in the diagrams even at ionic concentrations up to 1 M. Therefore, none of these M_2Xenes are predicted to be viable using aqueous etching, regardless of the acid or the precursor used. This also means that these M_2Xenes, even if synthesized by alternative means, are unsuitable for aqueous applications, including photocatalysis. Thicker and more stable n = 2 $Hf_3C_2O_2$ and $Zr_3C_2O_2$ MXenes, however, were recently synthesized by etching layered compounds similar to MAX phases.[39,40]

DOI: 10.1021/acs.jpcc.8b10802
J. Phys. Chem. C 2019, 123, 3180−3187

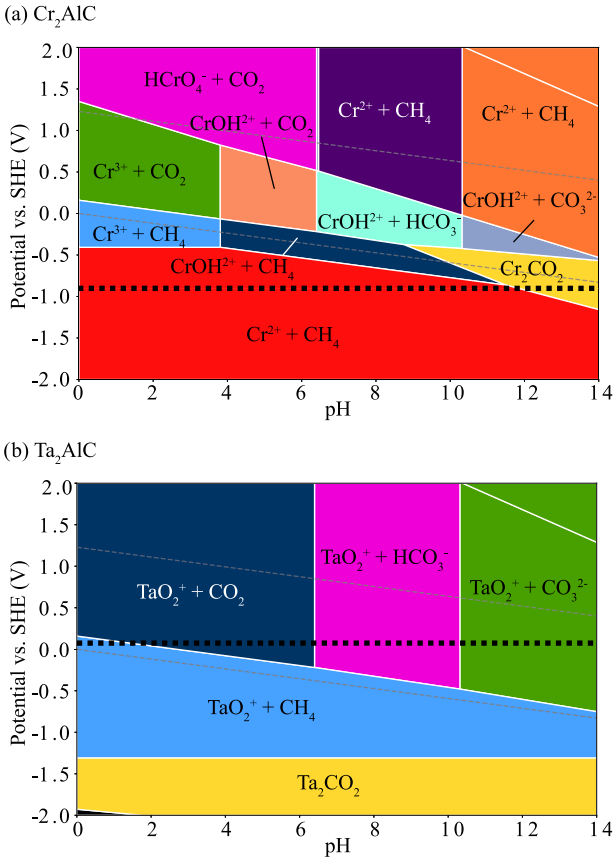

Figure 8. Etching diagrams for (a) Cr_2AlC and (b) Ta_2AlC and their respective M_2Xenes. The PZC values are shown by the dashed black lines.

■ CONCLUSIONS

We have developed a method by which the electrochemical synthesis of MXenes can be predicted using partial Pourbaix diagrams. This method can be generalized to apply to any class of materials under investigation as precursors for etching 2D materials or other metastable phases.

Specifically, the etching diagrams offer solution conditions that may enhance the yields of etching reactions of existing Ti_2CO_2 and V_2CO_2 M_2Xenes and may enable the synthesis of new M_2Xenes compounds, including Cr_2CO_2 and Ta_2CO_2. In general, we recommend preconditioning etching solutions with high concentrations of metallic ions to inhibit the dissolution of metallic M_2Xene surfaces and thereby increase the final M_2Xene yield.

Importantly, the diagrams generated for nitride M_2Xenes show that some are metastable in acidic solutions, but the A elements, e.g., Ga, in many of their experimentally available precursors are more difficult to etch than Al. This offers an explanation why nearly all MXenes have been electrochemically synthesized from A = Al precursors to date.

■ AUTHOR INFORMATION

Corresponding Author

*E-mail: rhennig@ufl.edu.

ORCID

Michael Ashton: 0000-0003-4600-5395

Richard G. Hennig: 0000-0003-4933-7686

Notes

The authors declare no competing financial interest.

■ ACKNOWLEDGMENTS

M.A. and S.B.S. gratefully acknowledge the support of the National Science Foundation under grant no. DMR-1307840. R.G.H. gratefully acknowledges the support of the National Science Foundation under grants DMR-1665310 and 1740251. The calculations were performed using the resources of the University of Florida's High Performance Computing Clusters.

■ REFERENCES

(1) Li, X.; Magnuson, C. W.; Venugopal, A.; Tromp, R. M.; Hannon, J. B.; Vogel, E. M.; Colombo, L.; Ruoff, R. S. Large-area graphene single crystals grown by low-pressure chemical vapor deposition of methane on copper. *J. Am. Chem. Soc.* **2011**, *133*, 2816−2819.

(2) Joensen, P.; Frindt, R.; Morrison, S. R. Single-layer MoS_2. *Mater. Res. Bull.* **1986**, *21*, 457−461.

(3) Lin, Y.; Williams, T. V.; Connell, J. W. Soluble, exfoliated hexagonal boron nitride nanosheets. *J. Phys. Chem. Lett.* **2010**, *1*, 277−283.

(4) Altuntasoglu, O.; Matsuda, Y.; Ida, S.; Matsumoto, Y. Syntheses of zinc oxide and zinc hydroxide single nanosheets. *Chem. Mater.* **2010**, *22*, 3158−3164.

(5) Ashton, M.; Mathew, K.; Hennig, R. G.; Sinnott, S. B. Predicted surface composition and thermodynamic stability of MXenes in solution. *J. Phys. Chem. C* **2016**, *120*, 3550−3556.

(6) Naguib, M.; Kurtoglu, M.; Presser, V.; Lu, J.; Niu, J.; Heon, M.; Hultman, L.; Gogotsi, Y.; Barsoum, M. W. Two-Dimensional Nanocrystals Produced by Exfoliation of Ti_3AlC_2. *Adv. Mater.* **2011**, *23*, 4248−4253.

(7) Zhuang, H. L.; Hennig, R. G. Computational discovery, characterization, and design of single-layer materials. *JOM* **2014**, *66*, 366−374.

(8) Ashton, M.; Hennig, R.; Sinnott, S. Computational Characterization of Lightweight Multilayer MXene Li-ion Battery Anodes. *Appl. Phys. Lett.* **2016**, *108*, No. 023901.

(9) Rasmussen, F. A.; Thygesen, K. S. Computational 2D materials database: electronic structure of transition-metal dichalcogenides and oxides. *J. Phys. Chem. C* **2015**, *119*, 13169−13183.

(10) Singh, A. K.; Revard, B. C.; Ramanathan, R.; Ashton, M.; Tavazza, F.; Hennig, R. G. Genetic algorithm prediction of two-dimensional group-IV dioxides for dielectrics. *Phys. Rev. B* **2017**, *95*, No. 155426.

(11) Paul, J.; Singh, A.; Dong, Z.; Zhuang, H.; Revard, B.; Rijal, B.; Ashton, M.; Linscheid, A.; Blonsky, M.; Gluhovic, D.; et al. Computational methods for 2D materials: discovery, property characterization, and application design. *J. Phys.: Condens. Matter* **2017**, *29*, No. 473001.

(12) Lebègue, S.; Björkman, T.; Klintenberg, M.; Nieminen, R. M.; Eriksson, O. Two-dimensional materials from data filtering and ab initio calculations. *Phys. Rev. X* **2013**, *3*, No. 031002.

(13) Ashton, M.; Paul, J.; Sinnott, S. B.; Hennig, R. G. Topology-scaling identification of layered solids and stable exfoliated 2D materials. *Phys. Rev. Lett.* **2017**, *118*, No. 106101.

(14) Singh, A. K.; Hennig, R. G. Computational synthesis of single-layer GaN on refractory materials. *Appl. Phys. Lett.* **2014**, *105*, No. 051604.

(15) Eichfeld, S. M.; Hossain, L.; Lin, Y.-C.; Piasecki, A. F.; Kupp, B.; Birdwell, A. G.; Burke, R. A.; Lu, N.; Peng, X.; Li, J.; et al. Highly scalable, atomically thin WSe_2 grown via metal-organic chemical vapor deposition. *ACS Nano* **2015**, *9*, 2080−2087.

(16) Persson, K. A.; Waldwick, B.; Lazic, P.; Ceder, G. Prediction of solid-aqueous equilibria: Scheme to combine first-principles calculations of solids with experimental aqueous states. *Phys. Rev. B* **2012**, *85*, No. 235438.

DOI: 10.1021/acs.jpcc.8b10802
J. Phys. Chem. C 2019, 123, 3180−3187

(17) Singh, A. K.; Mathew, K.; Zhuang, H. L.; Hennig, R. G. Computational Screening of 2D Materials for Photocatalysis. *J. Phys. Chem. Lett.* **2015**, *6*, 1087−1098.
(18) Naguib, M.; Mashtalir, O.; Carle, J.; Presser, V.; Lu, J.; Hultman, L.; Gogotsi, Y.; Barsoum, M. W. Two-dimensional transition metal carbides. *ACS Nano* **2012**, *6*, 1322−1331.
(19) Naguib, M.; Come, J.; Dyatkin, B.; Presser, V.; Taberna, P.-L.; Simon, P.; Barsoum, M. W.; Gogotsi, Y. MXene: a promising transition metal carbide anode for lithium-ion batteries. *Electrochem. Commun.* **2012**, *16*, 61−64.
(20) Tang, Q.; Zhou, Z.; Shen, P. Are MXenes promising anode materials for Li ion batteries? Computational studies on electronic properties and Li storage capability of Ti_3C_2 and $Ti_3C_2X_2$ (X = F, OH) monolayer. *J. Am. Chem. Soc.* **2012**, *134*, 16909−16916.
(21) Naguib, M.; Halim, J.; Lu, J.; Cook, K. M.; Hultman, L.; Gogotsi, Y.; Barsoum, M. W. New two-dimensional niobium and vanadium carbides as promising materials for Li-ion batteries. *J. Am. Chem. Soc.* **2013**, *135*, 15966−15969.
(22) Hu, Q.; Sun, D.; Wu, Q.; Wang, H.; Wang, L.; Liu, B.; Zhou, A.; He, J. MXene: A new family of promising hydrogen storage medium. *J. Phys. Chem. A* **2013**, *117*, 14253−14260.
(23) Ghidiu, M.; Naguib, M.; Shi, C.; Mashtalir, O.; Pan, L.; Zhang, B.; Yang, J.; Gogotsi, Y.; Billinge, S.; Barsoum, M. Synthesis and characterization of two-dimensional Nb_4C_3 (MXene). *Chem. Commun.* **2014**, *50*, 9517−9520.
(24) Naguib, M.; Mochalin, V. N.; Barsoum, M. W.; Gogotsi, Y. 25th anniversary article: MXenes: a new family of two-dimensional materials. *Adv. Mater.* **2014**, *26*, 992−1005.
(25) Lei, J.-C.; Zhang, X.; Zhou, Z. Recent advances in MXene: preparation, properties, and applications. *Front. Phys.* **2015**, *10*, 276−286.
(26) Jeitschko, W.; Nowotny, H.; Benesovsky, F. Carbides of formula T_2MC. *J. Less-Common Met.* **1964**, *7*, 133−138.
(27) Schuster, J.; Nowotny, H.; Vaccaro, C. The ternary systems: CrAlC, VAlC, and TiAlC and the behavior of H-phases (M_2AlC). *J. Solid State Chem.* **1980**, *32*, 213−219.
(28) Goto, T.; Hirai, T. Chemically vapor deposited Ti_3SiC_2. *Mater. Res. Bull.* **1987**, *22*, 1195−1201.
(29) Dahlqvist, M.; Alling, B.; Rosén, J. Stability trends of MAX phases from first principles. *Phys. Rev. B* **2010**, *81*, No. 220102.
(30) Ashton, M.; Hennig, R. G.; Broderick, S. R.; Rajan, K.; Sinnott, S. B. Computational discovery of stable M_2AX phases. *Phys. Rev. B* **2016**, *94*, No. 054116.
(31) Eklund, P.; Beckers, M.; Jansson, U.; Högberg, H.; Hultman, L. The $M_{n+1}AX_n$ phases: materials science and thin-film processing. *Thin Solid Films* **2010**, *518*, 1851−1878.
(32) Halim, J.; Lukatskaya, M. R.; Cook, K. M.; Lu, J.; Smith, C. R.; Näslund, L.-Å.; May, S. J.; Hultman, L.; Gogotsi, Y.; Eklund, P.; Barsoum, M. W. Transparent conductive two-dimensional titanium carbide epitaxial thin films. *Chem. Mater.* **2014**, *26*, 2374−2381.
(33) Ghidiu, M.; Lukatskaya, M. R.; Zhao, M.-Q.; Gogotsi, Y.; Barsoum, M. W. Conductive two-dimensional titanium carbide 'clay' with high volumetric capacitance. *Nature* **2014**, 78−81.
(34) Mashtalir, O.; Naguib, M.; Mochalin, V. N.; Dall'Agnese, Y.; Heon, M.; Barsoum, M. W.; Gogotsi, Y. Intercalation and delamination of layered carbides and carbonitrides. *Nat. Commun.* **2013**, *4*, No. 1716.
(35) Khazaei, M.; Arai, M.; Sasaki, T.; Chung, C.-Y.; Venkataramanan, N. S.; Estili, M.; Sakka, Y.; Kawazoe, Y. Novel electronic and magnetic properties of two-dimensional transition metal carbides and nitrides. *Adv. Funct. Mater.* **2013**, *23*, 2185−2192.
(36) Urbankowski, P.; Anasori, B.; Makaryan, T.; Er, D.; Kota, S.; Walsh, P. L.; Zhao, M.; Shenoy, V. B.; Barsoum, M. W.; Gogotsi, Y. Synthesis of two-dimensional titanium nitride Ti_4N_3 (MXene). *Nanoscale* **2016**, *8*, 11385−11391.
(37) Soundiraraju, B.; George, B. K. Two-dimensional titanium nitride (Ti_2N) MXene: synthesis, characterization, and potential application as surface-enhanced Raman scattering substrate. *ACS Nano* **2017**, *11*, 8892−8900.
(38) Meshkian, R.; Näslund, L.-Å.; Halim, J.; Lu, J.; Barsoum, M. W.; Rosen, J. Synthesis of two-dimensional molybdenum carbide, Mo_2C, from the gallium based atomic laminate Mo_2Ga_2C. *Scr. Mater.* **2015**, *108*, 147−150.
(39) Zhou, J.; Zha, X.; Chen, F. Y.; Ye, Q.; Eklund, P.; Du, S.; Huang, Q. A two-dimensional zirconium carbide by selective etching of Al_3C_3 from nanolaminated $Zr_3Al_3C_5$. *Angew. Chem.* **2016**, *128*, 5092−5097.
(40) Zhou, J.; Zha, X.; Zhou, X.; Chen, F.; Gao, G.; Wang, S.; Shen, C.; Chen, T.; Zhi, C.; Eklund, P.; et al. Synthesis and electrochemical properties of two-dimensional hafnium carbide. *ACS Nano* **2017**, *11*, 3841−3850.
(41) Ong, S. P.; Richards, W. D.; Jain, A.; Hautier, G.; Kocher, M.; Cholia, S.; Gunter, D.; Chevrier, V. L.; Persson, K. A.; Ceder, G. Python materials genomics (pymatgen): a robust, open-source python library for materials analysis. *Comput. Mater. Sci.* **2013**, *68*, 314−319.
(42) Mathew, K.; Singh, A. K.; Gabriel, J. J.; Choudhary, K.; Sinnott, S. B.; Davydov, A. V.; Tavazza, F.; Hennig, R. G. MPInterfaces: a Materials Project based python tool for high-throughput computational screening of interfacial systems. *Comput. Mater. Sci.* **2016**, *122*, 183−190.
(43) Wagman, D. D.; Evans, W. H.; Parker, V. B.; Schumm, R. H.; Halow, I.; et al. The NBS tables of chemical thermodynamic properties. Selected values for inorganic and C1 and C2 organic substances in SI units. *J. Phys. Chem. Ref. Data* **1989**, 1807−1812.
(44) Pourbaix, M. *Atlas of Electrochemical Equilibria in Aqueous Solutions*. National Association of Corrosion Engineers, Houston, Texas, 1974.
(45) Todorova, M.; Neugebauer, J. Extending the concept of defect chemistry from semiconductor physics to electrochemistry. *Phys. Rev. Appl.* **2014**, *1*, No. 014001.
(46) Kresse, G.; Hafner, J. Ab initio molecular dynamics for liquid metals. *Phys. Rev. B* **1993**, *47*, 558.
(47) Kresse, G.; Hafner, J. Ab initio molecular-dynamics simulation of the liquid-metal-amorphous-semiconductor transition in germanium. *Phys. Rev. B* **1994**, *49*, 14251.
(48) Monkhorst, H. J.; Pack, J. D. Special points for Brillouin-zone integrations. *Phys. Rev. B* **1976**, *13*, 5188.
(49) Zhang, D.; Ashton, M.; Ostadhossein, A.; van Duin, A. C.; Hennig, R. G.; Sinnott, S. B. Computational Study of Low Interlayer Friction in $Ti_{n+1}C_n$ (n= 1, 2, and 3) MXene. *ACS Appl. Mater. Interfaces* **2017**, *9*, 34467−34479.
(50) Dion, M.; Rydberg, H.; Schröder, E.; Langreth, D. C.; Lundqvist, B. I. Van der Waals density functional for general geometries. *Phys. Rev. Lett.* **2004**, *92*, No. 246401.
(51) Román-Pérez, G.; Soler, J. M. Efficient implementation of a van der Waals density functional: application to double-wall carbon nanotubes. *Phys. Rev. Lett.* **2009**, *103*, No. 096102.
(52) Klimeš, J.; Bowler, D. R.; Michaelides, A. Chemical accuracy for the van der Waals density functional. *J. Phys.: Condens. Matter* **2009**, *22*, No. 022201.
(53) Klimeš, J.; Bowler, D. R.; Michaelides, A. Van der Waals density functionals applied to solids. *Phys. Rev. B* **2011**, *83*, No. 195131.
(54) Kubaschewski, O.; Alcock, C. B.; Spencer, P. J. *Materials Thermochemistry*. Pergamon Press Ltd., New York, 1992.
(55) Mathew, K.; Sundararaman, R.; Letchworth-Weaver, K.; Arias, T.; Hennig, R. G. Implicit solvation model for density-functional study of nanocrystal surfaces and reaction pathways. *J. Chem. Phys.* **2014**, *140*, No. 084106.
(56) Mathew, K.; Hennig, R. G. Implicit Self-Consistent Description of Electrolyte in Plane-Wave Density-Functional Theory. 2016, *arXiv:1601.03346. arXiv.org e-Print archive.* https://arxiv.org/abs/1601.03346 (accessed Jan 13, 2016).
(57) Hu, C.; Lai, C.-C.; Tao, Q.; Lu, J.; Halim, J.; Sun, L.; Zhang, J.; Yang, J.; Anasori, B.; Wang, J.; et al. Mo_2Ga_2C: a new ternary nanolaminated carbide. *Chem. Commun.* **2015**, *51*, 6560−6563.
(58) Urbankowski, P.; Anasori, B.; Hantanasirisakul, K.; Yang, L.; Zhang, L.; Haines, B.; May, S. J.; Billinge, S. J.; Gogotsi, Y. 2D molybdenum and vanadium nitrides synthesized by ammoniation of

DOI: 10.1021/acs.jpcc.8b10802
J. Phys. Chem. C 2019, 123, 3180−3187

2D transition metal carbides (MXenes). *Nanoscale* **2017**, *9*, 17722−17730.

(59) Abdelmalak, M. N. *MXenes: A New Family of Two-Dimensional Materials and Its Application as Electrodes for Li-Ion Batteries*; Drexel University, 2014.

(60) Tian, W.; Vanmeensel, K.; Wang, P.; Zhang, G.; Li, Y.; Vleugels, J.; van der Biest, O. Synthesis and characterization of Cr_2AlC ceramics prepared by spark plasma sintering. *Mater. Lett.* **2007**, *61*, 4442−4445.

DOI: 10.1021/acs.jpcc.8b10802
J. Phys. Chem. C 2019, 123, 3180−3187